Stability Analysis of a Free-Falling Pararotor

Vicente Nadal-Mora / Ángel Sanz-Andrés

The pararotor is a decelerator device based on the autorotation of a rotating wing. When it is dropped, it generates an aerodynamic force parallel to the main motion direction, acting as a decelerating force. In this paper, the rotational motion equations are shown for the vertical flight without any lateral wind component and some simplifying assumptions are introduced to obtain analytic solutions of the motion. First, the equilibrium state is obtained as a function of the main parameters. Then the equilibrium stability is analyzed. The motion stability depends on two nondimensional parameters, which contain geometric, inertia, and aerodynamic characteristics of the device. Based on these two parameters a stability diagram can be defined. Some stability regions with different types of stability trajectories (nodes, spirals, focuses) can be identified for spinning motion around axes close to the major, minor, and intermediate principal axes. It is found that the blades contribute to stability in a case of spin around the intermediate principal inertia axis, which is otherwise unstable. Subsequently, the equations for determining the angles of nutation and spin of the body are obtained, thus defining the orientation of the body for a stationary motion and the parameters on which that position depends.

Nomenclature

A, B, C	=	principal moments of inertia
$a_{i,j}$	=	coefficients
b	=	blades span
b_i	=	coefficients
c	=	blades chord
c_D	=	drag coefficient of the blade
$c_{L\alpha}$	=	slope of the curve lift vs angle of attack for the blade
c_{mai}	=	aerodynamic moment coefficient components, $i = 1, 2, 3$
D	=	drag
$D_{i,j}$	=	drag component along j axis for blade i, $j = 1, 2, 3$; $i = 1, 2$
d	=	cylinder diameter
det	=	determinant
e	=	blades thickness
e_1, e_2, e_3	=	directions of the body-fixed axes
h	=	cylinder height
I_a	=	parameter that represents the moment of inertia of the air moving with the blades
i, j, k	=	directions of the inertial reference system axes
$k, k_{1,2}$	=	roots of the characteristic equation
k_{21}	=	ratio of coordinates of the center of pressure of the blade
k_A, k_B	=	relation of the moments of inertia
k_e	=	parameter used for the stability analysis
L	=	lift
L_i	=	lift for blade i, $i = 1, 2$
$L_{i,j}$	=	lift component along j axis for blade i,$j = 1, 2, 3$; $i = 1, 2$
l	=	distance between blades and body center of mass
M_a	=	moment of the aerodynamic forces
M_i	=	moment acting on the body, $i = 1, 2, 3$
N_e	=	stability number
$\bar{n}_i$	=	direction perpendicular to blade i surface, $i = 1, 2$
q_0	=	dynamic pressure
R	=	model radius
$\bar{r}_{Pi}$	=	representative point for the blade i, $i = 1, 2$
r_{pij}	=	component j of the vector position of the center of pressure of the blade i; $j = 1, 2, 3$; $i = 1, 2$
S	=	area of one blade
T	=	dimensionless time
t	=	time
t_c	=	characteristic time
tr	=	trace
U_∞	=	falling velocity
V_{rel}	=	relative velocity
X, Y, Z	=	inertial reference system
X_1, X_2	=	dimensionless variables used for the dynamic analysis
x_1, x_2	=	dimensionless angular velocities
x_{1e}, x_{2e}	=	dimensionless angular velocities at equilibrium
α	=	angle of attack
α_0	=	angle of attack related to the mean angle of incidence
α_1, α_2	=	angle of attack of blade 1, 2 (also coefficients used for the dynamic analysis)
β_0	=	mean angle of incidence
β_1, β_2	=	angle of incidence of blade 1, 2
Δ	=	discriminant
δ_β	=	pitch difference between the blades
θ	=	nutation angle
ρ	=	air density
ϕ	=	angle of incidence of the flow
φ	=	spin angle
	=	precession angle
ω	=	angular velocity
ω_0	=	angular velocity along the 3 axis
$\omega_1, \omega_2, \omega_3$	=	angular velocity components
1, 2, 3	=	body-fixed reference system

I. Introduction

THE purpose of this work is to study the dynamic behavior of a decelerating device based on the pararotor concept. The purpose of such a probe could be, for instance, the exploration of the

atmosphere and the measurement of the atmospheric conditions around airports for aviation operations support or the exploration of planetary atmospheres.

Actually, there are many devices that perform tasks such as measuring winds, emissions, and atmospheric parameters for aviation support. Each of them has their own advantages and drawbacks. There are not systems that could, on their own, measure all the parameters and cover the required three-dimensional space: radar, balloon, parachute, network of anemometers, etc. The pararotor could contribute to this set of systems with its own capabilities. Knowing the behavior of the pararotor, i.e., aerodynamics, dynamics, etc., it would be possible to know how to handle the system parameters to attain desired movement characteristics. As a result, it would be possible to know the place where the system could be inserted into the integrated terminal weather system.

The pararotor flies in the so-called autorotation regime. Aerodynamic forces are generated taking out energy from the fluid flow. These forces produce a fast rotation motion, a large rotation speed. This motion induces a large lift on the rotating blades, which is seen as a net aerodynamic drag acting on the body.

Although the autorotation regime is widely known for applications in helicopters, the problem studied here is different due to the small aspect ratio of the pararotor blades. In this case, the aspect ratio is about one, so the aerodynamic concepts developed for helicopters cannot be applied. For transportation requirements, the wings should be folded over the main body of the probe, which is cylindrical in shape, and the height of the body is limited for gyroscopic stability reasons, therefore, the aspect ratio is limited.

Before continuing, let us consider first the existing methods for decelerating the fall of bodies in the atmosphere reported in the literature. Parachutes are a widely known example. They have limitations that make it interesting to look for alternatives, like the use of wings or asymmetries to generate a rotation movement and thus lift in the rotating surfaces. That way, drag in the falling direction of the rotating body is increased and, sometimes, stability too. Balloons are widely used too for transportation of sensors to measure atmospheric parameters. They are cheap to operate and can carry heavy payloads at high altitudes, but they are slow and their trajectory is affected by lateral winds.

Among the studies performed concerning the deceleration and control of falling of bodies, there are those carried out by Shpund and Levin [1–4] in the area of rotating parachutes. Karlsen et al.[5] worked on winged bodies for submunition applications. They reported on the advantages of the pararotor over the parachute: lower sensitivity to lateral winds, parachute deployment problems, lower precession movements, and higher falling velocity.

The flight of samara wings has similarities with pararotors. Seter and Rosen [6,7] have studied numerically the influence of different parameters on samara flight stability. Crimi [8] has studied a rotating body with only one wing for submunition applications. He searched for a body that performed periodic movements. However, in these papers, there is no information about the behavior of a body with rotating wings like the one presented here and, to the authors' knowledge, there is no more closely related information in the literature.

The work performed and reported in this paper is structured as follows: in Sec. II, the motion equations for a cylindrical body with two identical blades that rotates and falls vertically at uniform velocity are developed, then a stability analysis is presented; in Sec. III, the allowed stability regions for spinning motion around axes close to the major, minor, and intermediate principal axes are described; in Sec. IV, the body attitude determination is shown; in Sec. V, a numerical example has been included; finally, conclusions on the results of the work are presented.

II. Mathematical Model. Rotational Motion Equations

The system analyzed consists of a cylindrical body with two identical blades that rotates at angular velocity $\bar{\omega}$ and falls vertically at uniform speed U_∞. The geometry is defined in Figs. 1 and 2. The body-fixed reference system 1, 2, 3 has its origin at the center of mass and directions e_1, e_2, e_3. The axes 1, 2, 3 are principal axes of the body. The inertial reference system is X, Y, Z; its axes have the directions i, j, k. The blades are located on the plane 1, 2.

Euler's equations are

$$\dot{\omega}_1 - \frac{B-C}{A}\omega_2\omega_3 = \frac{1}{A}M_1 \tag{1a}$$

$$\dot{\omega}_2 + \frac{A-C}{B}\omega_1\omega_3 = \frac{1}{B}M_2 \tag{1b}$$

$$\dot{\omega}_3 - \frac{A-B}{C}\omega_1\omega_2 = \frac{1}{C}M_3 \tag{1c}$$

The aerodynamic forces that act over the blades 1 and 2 can be written as

$$\frac{\bar{L}_1}{q_0 S c_{L\alpha}} \simeq \left(-\beta_1 + \frac{\omega_2}{\omega_3} + \phi\right)\begin{Bmatrix} 0 \\ \phi + \omega_2/\omega_3 \\ 1 \end{Bmatrix} \tag{2a}$$

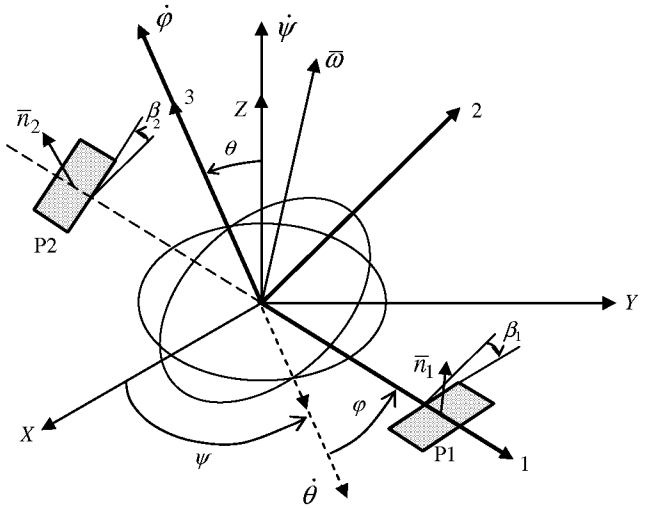

Fig. 1 System geometry. X, Y, Z, inertial reference system; 1, 2, 3, body-fixed reference system; ψ, precession angle; θ, nutation angle; φ, spin angle; $\bar{\omega}$, angular velocity.

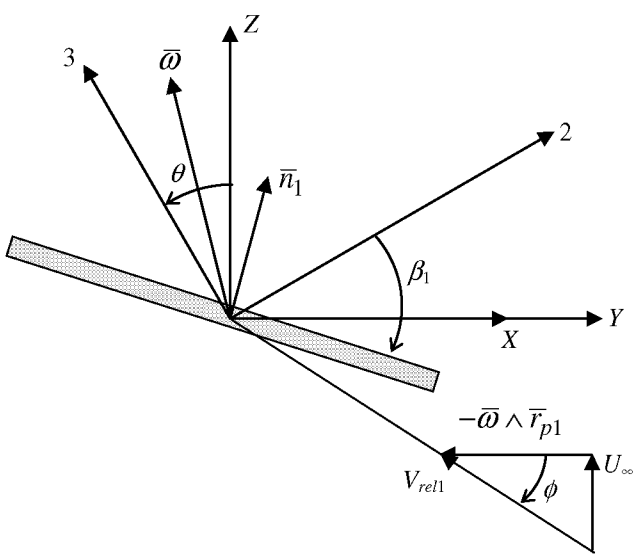

Fig. 2 P1 blade, as seen from the 1 axis.

$$\frac{\bar{L}_2}{q_0 S c_{L\alpha}} \simeq \left(-\beta_2 - \frac{\omega_2}{\omega_3} + \phi\right)\begin{Bmatrix} 0 \\ \omega_2/\omega_3 - \phi \\ 1 \end{Bmatrix} \tag{2b}$$

$$\frac{\bar{D}_1}{q_0 S} \simeq c_D(\alpha_1)\begin{Bmatrix} 0 \\ -1 \\ \frac{\omega_2}{\omega_3} + \phi \end{Bmatrix} \tag{2c}$$

$$\frac{\bar{D}_2}{q_0 S} \simeq c_D(\alpha_2)\begin{Bmatrix} 0 \\ 1 \\ \phi - \frac{\omega_2}{\omega_3} \end{Bmatrix} \tag{2d}$$

The determination of these expressions is too tedious to be included here. However, the readers interested in the details could ask directly to the authors or consult Ref. [9].

To obtain these equations, the following assumptions were considered: 1) the angles of attack, the angle of incidence of the blade and of the flow are all small; and 2) the component along the 1 axis of the relative velocity to the blade does not have an aerodynamic influence. Also, the effect of the higher order terms has been neglected.

The moment of the aerodynamic forces is

$$\bar{M}_a = \begin{Bmatrix} r_{p12}(L_{13} + D_{13} - L_{23} - D_{23}) \\ -r_{p11}(L_{13} + D_{13} - L_{23} - D_{23}) \\ r_{p11}(L_{12} + D_{12} - L_{22} - D_{22}) \end{Bmatrix} \tag{3}$$

where r_{pij} is the coordinate of the center of pressure for blade i along j axis. By symmetry, $r_{p11} = -r_{p21}$ and $r_{p12} = -r_{p22}$. L_{ij} is the lift component along j axis acting on blade i. In the same way, D_{ij} is the drag component along j axis acting on blade i. The center of pressure for blade 1 is determined by $\bar{r}_{P1} = (r_{p11}, 0, 0)$.

By using the preceding simplifying assumptions, the equations of rotational motion around the center of mass for the vertical free falling pararotor are

$$\dot{\omega}_1 - \frac{B-C}{A}\omega_2\omega_3 = \frac{1}{A} r_{p11} q_0 S c_{\mathrm{ma1}} = k_A^{-1}\frac{1}{t_c^2 2 c_{L\alpha}} c_{\mathrm{ma1}} = -\frac{k_A^{-1}}{t_c^2} k_{21}\left(\delta_\beta - \frac{\omega_2}{\omega_3}\right) \tag{4a}$$

$$\dot{\omega}_2 + \frac{A-C}{B}\omega_1\omega_3 = \frac{1}{B} r_{p11} q_0 S c_{\mathrm{ma2}} = k_B^{-1}\frac{1}{t_c^2 2 c_{L\alpha}} c_{\mathrm{ma2}} = \frac{k_B^{-1}}{t_c^2}\left(\delta_\beta - \frac{\omega_2}{\omega_3}\right) \tag{4b}$$

$$\dot{\omega}_3 - \frac{A-B}{C}\omega_1\omega_2 = \frac{1}{C} r_{p11} q_0 S c_{\mathrm{ma3}} = \frac{1}{t_c^2 2 c_{L\alpha}} c_{\mathrm{ma3}} = \frac{1}{t_c^2}\left[\phi\alpha_0 + \frac{\omega_2}{\omega_3}\left(\frac{\omega_2}{\omega_3} - \delta_\beta\right) - \frac{c_D(\alpha_0)}{c_{L\alpha}}\right] \tag{4c}$$

where:

$$\beta_1 = \beta_0 + \delta_\beta \qquad \beta_2 = \beta_0 - \delta_\beta \qquad \alpha_0 = \phi - \beta_0$$
$$k_A = \frac{A}{C}; \qquad k_B = \frac{B}{C}; \qquad k_{21} = \frac{r_{p12}}{r_{p11}} \tag{5}$$
$$t_c^2 = \frac{C}{2 c_{L\alpha} r_{p11} q_0 S} = \frac{C}{2 c_{L\alpha} r_{p11} S \frac{1}{2}\rho (r_{p11}\omega_0)^2} = \frac{C}{c_{L\alpha} I_a \omega_0^2}$$

and $I_a = \rho S r_{p11}^3$ is a parameter that represents the moment of inertia of the air mass influenced by the blade motion. The characteristic time t_c associated to the moment of the aerodynamic forces indicates that the evolution for one given configuration is faster as ω_0 increases ($\omega_0 = \omega_3$).

With further assumptions, Eq. (4c) can be uncoupled from the others. Actually, it is known from the experiments that ω_3 is constant, $\omega_3 = \omega_0$, where ω_0 is the solution of Eq. (4c) when $\dot{\omega}_3 = 0$ and ω_1, $\omega_2 \ll 1/t_c^2$. Therefore, the first two Eqs. (4a) and (4b) can be solved together, separated from the third. The system can be written as follows

$$\frac{B-C}{A}\frac{\omega_2}{\omega_0} = \frac{k_A^{-1} k_{21}}{t_c^2 \omega_0^2}\left(\delta_\beta - \frac{\omega_2}{\omega_0}\right) \tag{6a}$$

$$\frac{A-C}{B}\frac{\omega_1}{\omega_0} = \frac{k_B^{-1}}{t_c^2 \omega_0^2}\left(\delta_\beta - \frac{\omega_2}{\omega_0}\right) \tag{6b}$$

Defining the coefficients

$$\begin{gathered} a_{11} = 0 \qquad a_{12} = (B-C)/A + k_{21}/(k_A t_c^2 \omega_0^2) \\ a_{21} = (A-C)/B \qquad a_{22} = 1/(k_B t_c^2 \omega_0^2) = I_a c_{L\alpha}/B \\ b_1 = k_{21}/(k_A t_c^2 \omega_0^2)\delta_\beta = (I_a c_{L\alpha} k_{21}/A)\delta_\beta \\ b_2 = 1/(k_B t_c^2 \omega_0^2)\delta_\beta = (I_a c_{L\alpha}/B)\delta_\beta \end{gathered} \tag{7}$$

and defining the variables $x_1 = \omega_1/\omega_0$ and $x_2 = \omega_2/\omega_0$, and calling $t = T/\omega_0$, ($\dot{x} = \mathrm{d}x/\mathrm{d}t = \omega_0 \mathrm{d}x/\mathrm{d}T = \omega_0 x'$), the Eqs. (4a) and (4b) can finally be written as follows

$$\begin{cases} x_1' - a_{12} x_2 = -b_1 \\ x_2' + a_{21} x_1 + a_{22} x_2 = b_2 \end{cases} \tag{8}$$

The solution for the equilibrium is

$$x_2 = x_{2e} = b_1/a_{12} = \delta_\beta N_e/(N_e - 1) \tag{9a}$$

$$x_1 = x_{1e} = \frac{b_2}{a_{21}}\left(1 - \frac{a_{22}}{a_{12}}\frac{b_1}{b_2}\right) = -\frac{\delta_\beta}{k_{21}}\frac{C-B}{C-A}\frac{N_e}{1-N_e} \tag{9b}$$

where $N_e = I_a c_{L\alpha} k_{21}/(C-B)$ is called the "stability number." When $N_e \to 1$, there exists a divergence in the position of equilibrium, except that $\delta_\beta = 0$.

A. Stability Analysis

The stability is analyzed by following the classical method. New variables are defined

$$x_1 = x_{1e} + X_1$$

$$x_2 = x_{2e} + X_2$$

and from Eq. (8) the following system of equations is obtained:

$$\begin{cases} X_1' - a_{12} X_2 = 0 \\ X_2' + a_{21} X_1 + a_{22} X_2 = 0 \end{cases} \tag{10}$$

The solution for the autonomous system Eq. (10) is

$$\begin{cases} X_1 = \alpha_1 e^{kT} \\ X_2 = \alpha_2 e^{kT} \end{cases}$$

The determinant of the system is

$$\begin{vmatrix} k & -a_{12} \\ a_{21} & a_{22} + k \end{vmatrix} = 0$$

The stability is analyzed from the characteristic equation

$$k^2 + a_{22} k + a_{12} a_{21} = 0 \tag{11}$$

where $\mathrm{tr} = -a_{22}$, $\det = a_{12} a_{21}$, and $\Delta = \mathrm{tr}^2 - 4\det$.

The values of the roots of Eq. (11) are

$$k_{1,2} = \frac{1}{2}\left[-\frac{1}{k_B t_c^2 \omega_0} \pm \sqrt{\left(\frac{1}{k_B t_c^2 \omega_0}\right)^2 - 4\left(\frac{B-C}{A} + \frac{k_{21}}{k_A t_c^2 \omega_0^2}\right)\left(\frac{A-C}{B}\right)}\right] \quad (12)$$

which define the evolution of the trajectories of the system, either stable or unstable nodes, focuses, or spirals. The following cases appear [10]:

1) A stable node is given when $k_1 < 0$ and $k_2 < 0$, $k_{1,2}$ are real and different, tr < 0, det > 0, and $\Delta > 0$.

2) A stable spiral is given when $k_{1,2} = p \pm qi$, $p < 0$, $q \neq 0$, tr < 0, and $\Delta < 0$.

3) A stable focus is given when $k_1 = k_2 < 0$, tr < 0, and det $= 0$.

The stability limits are tr $= 0$ and det $= 0$.

1. Stable Node

To attain this condition, the Routh–Hurwitz criteria must be satisfied

$$-\text{tr} = a_{22} = 1/(k_B t_c^2 \omega_0^2) = c_{L\alpha} I_a / B > 0 \quad (13)$$

$$\det = a_{12} a_{21} = \left(\frac{B-C}{A} + \frac{k_{21}}{k_A t_c^2 \omega_0^2}\right)\left(\frac{A-C}{B}\right) > 0 \quad (14)$$

provided that $\Delta > 0$.

As by definition it is $A, B > 0$, Eq. (14) can be written as

$$(C-B)(C-A)(1-N_e) > 0 \quad (15)$$

If $C > A, B$, it must be $N_e < 1$ to fulfill the condition given by Eq. (15). As $I_a \ll C, B$, then $N_e \ll 1$ and that condition is satisfied in a general case, except when C is very close to B. In such a case, it can happen that $I_a \cong C - B$ and then $N_e = O(1)$, and a risk for instability appears.

The condition given by Eq. (13) is always satisfied. In the stability limit tr $= 0$, the trajectory is a center, and that occurs when $1/(k_B t_c^2 \omega_0^2) = c_{L\alpha} I_a / B = 0$; it should be $c_{L\alpha} = 0$. This last situation coincides with the classical problem of a rotating body in vacuum.

2. Stable Spiral

This case occurs when $\Delta < 0$. This condition can be written as

$$\frac{(C-B)^2}{k_{21}^2 B^2}[N_e^2 - k_e(1-N_e)] < 0 \quad (16)$$

where $k_e = 4k_{21}^2 \frac{B}{A}\frac{C-A}{C-B}$ is the so-called ratio of the moments of inertia in what follows.

It always happens that $(C-B)^2/k_{21}^2 B^2 > 0$, then, to attain a spiral trajectory, the condition $N_e^2 - k_e(1-N_e) < 0$ must be fulfilled.

3. Stable Focus

This type of trajectory will arise when the condition

$$N_e^2 - k_e(1-N_e) = 0 \quad (17)$$

is fulfilled and, therefore, the roots become $k_1 = k_2 = -1/(2k_B t_c^2 \omega_0)$; it is the solution in the limit $\Delta = 0$.

III. Stability Regions

As the signs of the differences of moments of inertia have an influence in the stability limits, their relative value should be taken into account. The results of this comparison are shown in the plane N_e, k_e parameters which define the stability regions. The following cases appear.

A. Spinning Motion Close to the Major Axis of Inertia. Inertial Stability.

In this case, $A, B < C$, so according to Eq. (15), the stability region is defined by the condition $N_e < 1$. Furthermore, as $B < C$, so is $N_e > 0$, and as $B < C$ and $A < C$, is $k_e > 0$, and so only the first quadrant of the plane N_e, k_e is allowed.

The limit for the region of spirals (focuses) is given by $N_e^2 - k_e(1-N_e) = 0$. Then, $k_e = N_e^2/(1-N_e)$ and the region of spirals is attained when $k_e > N_e^2/(1-N_e)$. These conditions are shown in Fig. 3.

When $N_e > 1$ (high aerodynamic effects in relation to $C - B$), the system is unstable. This situation does not happen when there are no aerodynamic forces over the body, that is, in the classical problem of a solid body rotating in a vacuum, whose motion is stable under the condition $A, B < C$.

B. Spinning Motion Close to the Axis of Lower Inertia. Inertial Stability.

In this case, $A, B > C$ and, therefore, $N_e < 0$ and $k_e > 0$. And so, only the second quadrant of the plane N_e, k_e is allowed [see condition given by Eq. (15)]. This situation is shown in Fig. 4.

When $N_e = 0$, the system follows a center-type evolution. This condition corresponds to a system without aerodynamic forces $c_{L\alpha} = 0$.

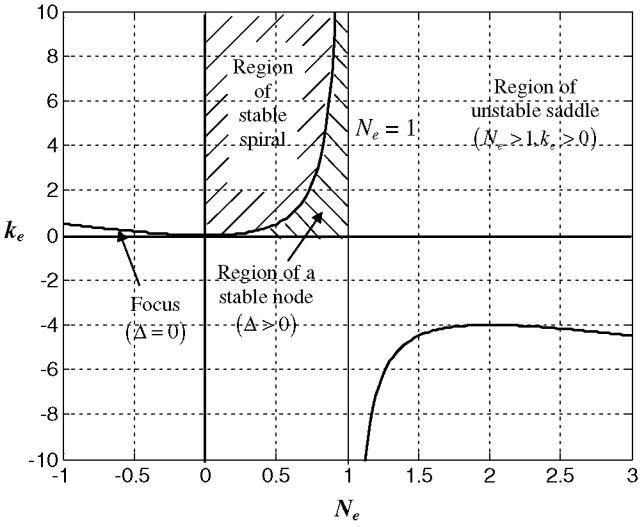

Fig. 3 Types of trajectories for the case $A, B < C$. Only the first quadrant is allowed.

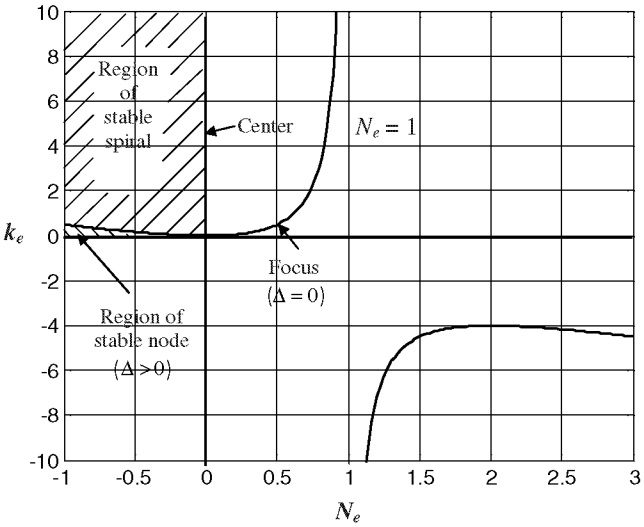

Fig. 4 Types of trajectories for $A, B > C$. Only the second quadrant is allowed.

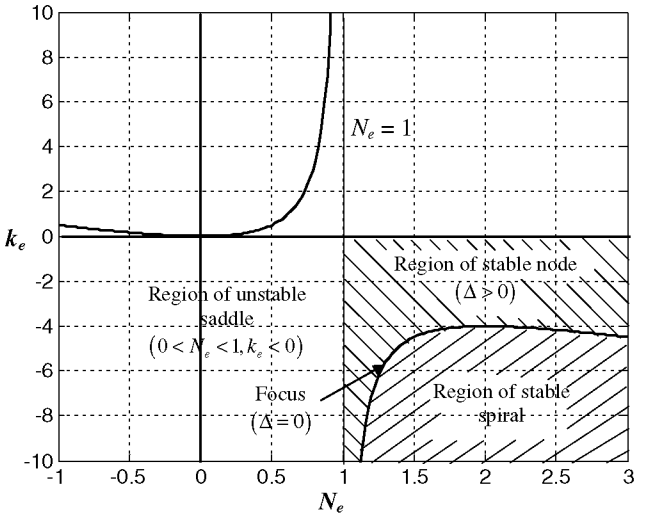

Fig. 5 Types of trajectories for $B < C < A$. Only the fourth quadrant is allowed.

C. Spinning Motion Close to the Axis of Intermediate Inertia. Case a) $B < C < A$. Aerodynamic Stabilization.

According to Eq. (15), the condition $N_e > 1$ must hold for a stable system. Furthermore, by definition $N_e > 0$ and $k_e < 0$, therefore, only the fourth quadrant of the plane N_e, k_e is allowed. The region of spirals is $k_e < -N_e^2/(N_e - 1)$, as shown in Fig. 5.

At the limit of the region of spirals, the maximum value of k_e occurs when $N_e = 2$ [Eq. (17)] and is $k_e = -4$.

The condition $N_e > 1$ is fulfilled whenever B is both lower than and close enough to C, depending also on the values of the other parameters involved in the definition of N_e.

Therefore, under specific conditions, the system can be stable when it is spinning around an axis close to the intermediate inertia axis. This is because of the stabilizing effect of the aerodynamic forces generated by the blades. Without that contribution the system would be unstable, as it is in the case of rotation in a vacuum.

D. Spinning Motion Close to the Axis of Intermediate Inertia. Case b) $A < C < B$. No Stability.

In this case, only the third quadrant of the plane is allowed $N_e < 0$ and $k_e < 0$. However, since according to Eq. (15), the condition $N_e > 1$ must be fulfilled for stable motion, there is no stable region allowed.

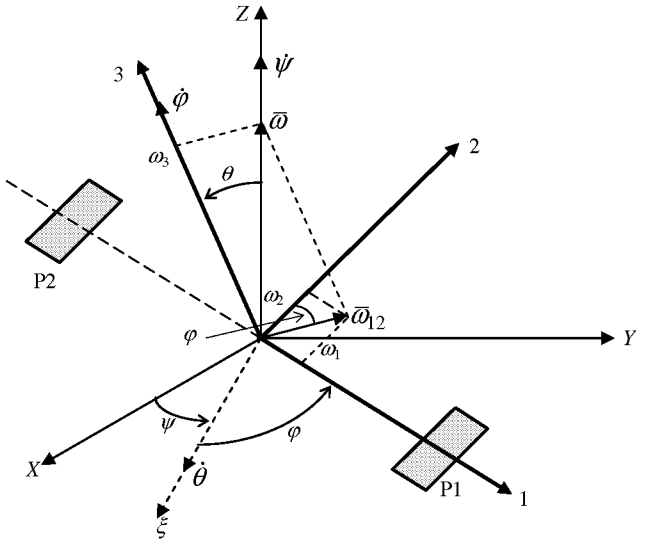

Fig. 6 Orientation of the body. X, Y, Z, inertial reference system; 1, 2, 3, body-fixed reference system; ψ, precession angle; θ, nutation angle; φ, spin angle. The angular velocity $\bar{\omega}$ has the Z axis direction.

IV. Determination of Body Attitude

The nutation angle θ and spin angle φ (Fig. 1) are determined as follows. The components of the angular velocity $\bar{\omega}$ in the body-fixed axes are given by the expressions

$$\omega_1 = \dot{\psi}\sin\theta\sin\varphi + \dot{\theta}\cos\varphi \tag{18a}$$

$$\omega_2 = \dot{\psi}\sin\theta\cos\varphi - \dot{\theta}\sin\varphi \tag{18b}$$

$$\omega_3 = \dot{\varphi} + \dot{\psi}\cos\theta \tag{18c}$$

For stationary motion, a velocity of nutation is not observed $\dot{\theta} = 0$, therefore, the equation system is reduced to

$$\omega_1 = \dot{\psi}\sin\theta\sin\varphi \tag{19a}$$

$$\omega_2 = \dot{\psi}\sin\theta\cos\varphi \tag{19b}$$

$$\omega_3 = \dot{\varphi} + \dot{\psi}\cos\theta \tag{19c}$$

From Eqs. (19a) and (19b), the rotation speed component in the 1–2 plane is given by

$$\omega_{12} = \sqrt{\omega_1^2 + \omega_2^2} = \dot{\psi}\sin\theta \tag{20}$$

and the spin angle

$$\tan\varphi = \omega_1/\omega_2 \tag{21}$$

Obviously, for the stationary case, ω_1 and ω_2 are constants. Therefore, from Eq. (21) it results that φ remains constant and $\dot{\varphi} = 0$. Then, from Eq. (19c), it follows that

$$\omega_3 = \dot{\psi}\cos\theta \tag{22}$$

From Eqs. (20) and (22), it is obtained

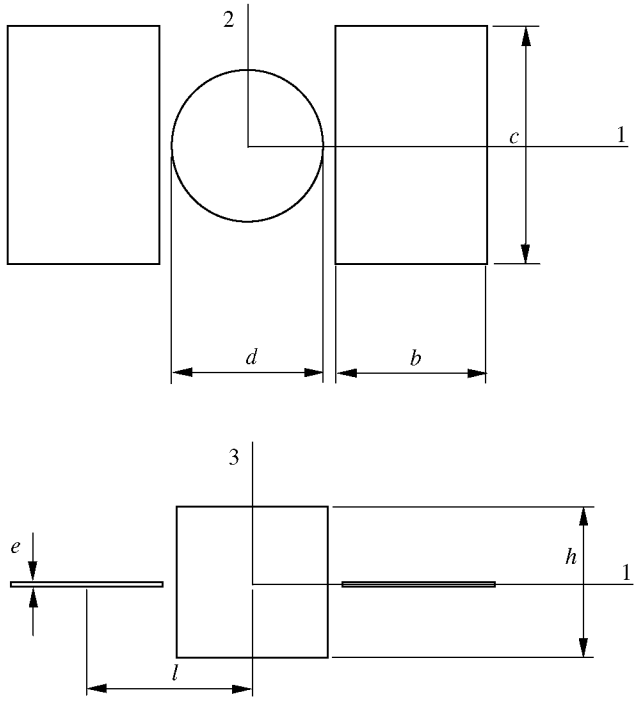

Fig. 7 Upper and side views of the model with dimensions and nomenclature.

Table 1 Model dimensions and inertia moments (nomenclature in Fig. 7)

	Body dimensions, m						Inertia moments, 10^4 kg · m^2		
Case	d	h	b	c	e	l	A	B	C
A, $B < C$	0.1	0.05	0.1	0.1	0.001	0.1	9	15	20
A, $B > C$	0.1	0.2	0.1	0.1	0.001	0.1	168	174	59
$B < C < A$	0.04	0.06	0.02	0.18	0.001	0.04	1.34	1.13	1.25

Table 2 Model stability analysis

	Motion stability parameters		Stability regions attained, trajectory type
Case	N_e	k_e	
A, $B < C$	0.026	0.69	1st quadrant, stable spiral
A, $B > C$	−0.001	0.203	2nd quadrant, stable spiral
$B < C < A$	0.110	−2.942	4th quadrant, unstable saddle

$$\tan\theta = \omega_{12}/\omega_3 \tag{23}$$

From Eqs. (21) and (23), it follows that $\bar{\omega}$ is a vector along the Z axis direction, as it is shown in Fig. 6. Then, the motion of the body is just pure precession ($\dot{\psi} \neq 0, \dot{\varphi} = \dot{\theta} = 0$) at a constant speed, given by $\dot{\psi} = \omega_3/\cos\theta$.

Substituting Eqs. (6a) and (6b) in Eq. (21), the spin angle is obtained from Eq. (21)

$$\tan\varphi = \frac{\omega_1}{\omega_2} = \frac{1}{k_{21}}\frac{B-C}{A-C} \tag{24}$$

where it is also seen that the spin angle is kept constant and depends only on the mass distribution and the position of the blades, and does not depend on the pitch difference between the blades δ_β.

From the solution for the equilibrium, Eqs. (9) and (10), the nutation angle can be obtained by

$$\begin{aligned}\tan\theta &= I_a c_{L\alpha}\frac{\delta_\beta}{N_e - 1}\sqrt{\frac{1}{(C-A)^2} + \frac{k_{21}^2}{(C-B)^2}} \\ &= -\left(\frac{N_e}{1-N_e}\right)\delta_\beta\sqrt{1 + \frac{1}{k_{21}^2}\left(\frac{C-B}{C-A}\right)^2} \\ &= -\left(\frac{N_e}{1-N_e}\right)\delta_\beta\sqrt{1+\tan^2\varphi} = -\left(\frac{N_e}{1-N_e}\right)\frac{\delta_\beta}{|\cos\varphi|}\end{aligned} \tag{25}$$

It is deduced that, for small angles of nutation, the nutation angle is proportional to the pitch difference between the blades δ_β.

The Eqs. (21) and (23) could be used also in the nonsteady case (small motions around the equilibrium position) if $\dot{\theta}$ and $\dot{\varphi}$ are small enough compared with the other terms in Eq. (18).

V. Numerical example

A numerical example of the stability analysis and body attitude determination is presented in this section. To develop it, an aluminum solid body composed of both a cylinder and blades with different relative dimensions, which produce different relations between the principal moments of inertia, is considered. A scheme of the body is shown in Fig. 7 and the model dimensions used for the example are summarized in Table 1.

Assuming that the center of pressure lies on 25% of the chord and 60% of the span of the blades [9], and that $\rho = 1.22$ Kg/m^3 and $c_{L\alpha} = 3.4$ [9], the motion stability parameters N_e and k_e are obtained and the allowed stability regions and trajectory types are determined (Table 2).

Table 3 Body attitude.

Case	φ, degrees	θ, degrees
A, $B < C$	64.3	−0.12
A, $B > C$	77.7	0.01
$B < C < A$	−50.9	0.35

To determine the body attitude, a pitch difference between the blades $\delta_\beta = 2°$ is assumed. The spin and nutation angles analyzed in the preceding three cases are shown in Table 3.

VI. Conclusions

As it is mentioned in preceding sections, the motion equations for the free falling pararotor have been obtained and the motion stability analyzed. From this last analysis, the following conclusions can be drawn:

1) Depending on the inertia axis, close to which the body spins, different types (nodes, spirals, focuses) of stability appear at different regions of the stability diagram.

2) The aerodynamic forces acting on the blades contribute to stability in the case of spin close to the intermediate inertia axis $B < C < A$, but when $A < C < B$, there is no stable region allowed.

From the determination of the position of the body by the angles of nutation and spin, it can be concluded that

1) The rotation speed vector $\bar{\omega}$ follows the inertial Z axis direction and the motion of the body is just pure precession at a constant speed.

2) The spin angle is kept constant and depends only on the mass distribution and the position of the blades and (in a first approximation) does not depend on the pitch difference between the blades δ_β.

3) For small angles of nutation, the nutation angle is proportional to the pitch difference between the blades δ_β. If $\delta_\beta = 0$, there is no nutation angle, and so the 3 axis follows the inertial Z axis direction.

4) For a given body, δ_β could be determined to obtain a given body attitude (nutation angle) that could be useful for a desired application. The changes in δ_β do not modify the spin angle.

5) In wind tunnel tests, it was observed that the drag in the falling direction decreases as the nutation angle increases [11], and so for a given body, δ_β could also be used to modify the falling speed.

References

[1] Shpund, Z., and Levin, D., "Measurement of the Static and Dynamic Coefficients of a Cross-Type Parachute in Subsonic Flow," *11th AIAA Aerodynamic Decelerator Systems Technology Conference*, AIAA Paper 91-0871, Washington, DC, 1991, pp. 295–303.

[2] Levin, D., and Shpund, Z., "Dynamic Investigation of the Angular Motion of a Rotating Body-Parachute System," *Journal of Aircraft*, Vol. 32, No. 1, 1995, pp. 93–99.

[3] Shpund, Z., and Levin, D., "Forebody Influence on Rotating Parachute Aerodynamic Properties," *Journal of Aircraft*, Vol. 34, No. 2, 1997, pp. 181–186.

[4] Levin, D., and Shpund, Z., "Canopy Geometry Effect on the Aerodynamic Behaviour of Cross-Type Parachutes," *Journal of Aircraft*, Vol. 34, No. 5, 1997, pp. 648–652.

[5] Karlsen, L., Borgström, D., and Paulsson, L., "Aerodynamics of a Rotating Body Descending from the Separation Position of an Artillery Munition Shell," *11th AIAA Aerodynamic Decelerator Systems Technology Conference*, AIAA Paper 91-870, Washington, DC, 1991, pp. 288–294.

[6] Rosen, A., and Seter, D., "Vertical Autorotation of a Single Winged Samara," *Transactions of the ASME*, Vol. 58, Dec. 1991, pp. 1064–1070.

[7] Seter, D., and Rosen, A., "Stability of the Vertical Autorotation of a Single Winged Samara," *Journal of Applied Mechanics*, Vol. 59, No. 4, Dec. 1992, pp. 1000–1008.

[8] Crimi, P., "Analysis of Samara-Wing Decelerator Steady-State Characteristics," *Journal of Aircraft*, Vol. 25, No. 1, 1988, pp. 41–47.

[9] Nadal Mora, V., "Comportamiento Aerodinámico de Sondas Atmosféricas en Entornos Aeroportuarios," Tesis Doctoral, Universidad Politécnica de Madrid, España, May 2005.

[10] Elsgoltz, L., *Teoría de la Estabilidad, Ecuaciones Diferenciales y Cálculo Variacional*, 2nd ed., MIR, Moscú, 1977, pp. 207–219.

[11] Sanz Andrés, A., Nadal Mora, V., and Cuerva, A., "Experimental Investigation of an Autorotating-Wing Aerodynamic Decelerator System," *18th AIAA Aerodynamic Decelerator Systems Technology Conference and Seminar*, AIAA Paper 2005-1635, 23–26 May, 2005.